



# Evidence for the predictability of changes in the stratospheric aerosol size following volcanic eruptions of diverse magnitudes using space-based instruments

Larry W. Thomason<sup>1</sup>, Mahesh Kovilakam<sup>2</sup>, Anja Schmidt<sup>3,4</sup>, Christian von Savigny<sup>5</sup>, Travis Knepp<sup>1</sup>,  
5 Landon Rieger<sup>6</sup>

<sup>1</sup>NASA Langley Research Center, Hampton, Virginia 23681 USA

<sup>2</sup>SSAI, Hampton, Virginia, USA

<sup>3</sup>Department of Chemistry, Cambridge University, Cambridge, UK

<sup>4</sup>Department of Geography, Cambridge University, Cambridge, UK

10 <sup>5</sup>Institute of Physics, University of Greifswald, Greifswald, Germany

<sup>6</sup>University of Saskatchewan, Saskatoon, Saskatchewan, Canada

*Correspondence to:* Larry W. Thomason (l.w.thomason@nasa.gov)

**Abstract.** An analysis of multiwavelength stratospheric aerosol extinction coefficient data from the Stratospheric Aerosol and Gas Experiment II and III/ISS instruments is used to demonstrate a coherent relationship between the perturbation in extinction  
15 coefficient in an eruption's main aerosol layer and an apparent change in aerosol size distribution that spans multiple orders of magnitude in the stratospheric impact of a volcanic event. The relationship is measurement-based and does not rely on assumptions about the aerosol size distribution. We note limitations on this analysis including that the presence of significant amounts of ash in the main aerosol layer may significantly modulate these results. Despite this limitation, these findings represent a unique opportunity to verify the performance of interactive aerosol models used in Global Climate Models and  
20 Earth System Model and may suggest an avenue for improving aerosol extinction coefficient measurements from single channel observations such the Optical Spectrograph and Infrared Imager System as they rely on a priori assumptions about particle size.

## 1 Introduction

Eruptions by volcanoes represent the primary source of variation in stratospheric aerosol levels (Thomason et al.,  
25 1997b; Solomon et al., 2011; Schmidt et al., 2018). Volcanically-derived aerosol is known for its ability to significantly modulate climate (Schmidt and Robock, 2015) primarily by scattering incoming solar radiation to space and even relatively small volcanic events have been noted to affect global temperature trends (Santer et al., 2014). In addition, since sulfuric acid aerosol particles absorb upwelling infrared radiation, the presence of a volcanic aerosol layer can change the thermal structure of the stratosphere and the troposphere and modulate stratospheric circulation as well as transport across the tropopause (Tang  
30 et al., 2013). Significant effort has been expended toward measuring stratospheric aerosol by a variety of instruments (Kremser et al., 2016). Global Climate Models (GCMs) and Earth System Models (ESMs) use either these measurements (Mann, 2015)



or interactive aerosol model schemes (Mills et al., 2016) and similar tools (Toohey et al., 2016) to infer the climate impact of historical and hypothetical volcanic injections of stratospheric aerosol and its precursors. Herein, we discuss observations made by the Stratospheric Aerosol and Gas Experiment (SAGE) II (1984-2005) and III/ISS (2017-present) which span a broad  
35 range of volcanic perturbations of the stratosphere. We demonstrate that, for the most part, the changes in aerosol extinction coefficient and apparent aerosol particle size are well correlated across nearly 2 orders of magnitude in extinction coefficient change. This relationship is a directly measurable characteristic of the changes in aerosol size distribution following an eruption without assumptions regarding the functional form for the aerosol size distribution (e.g., log-normal). Since comparisons of interactive aerosol model scheme calculations and measurements of stratospheric aerosol form the basis of  
40 assessing the performance of these aerosol microphysics modules, the observed relationship provides a potentially unique, measurement-focused means for assessing interactive aerosol models for volcanic eruptions of different magnitudes.

## 2 The measurements

Space-based measurements of stratospheric aerosol have been made on a nearly global basis since the Stratospheric Aerosol and Gas Experiment (SAGE) aboard the Applications Explorer Mission 2 platform operated from 1979 through 1981 (Chu  
45 and McCormick, 1979). The well-known SAGE II mission spanned the recovery of stratospheric aerosol levels from two large magnitude volcanic eruptions: the eruption of El Chichón in 1982 and the 1991 eruption of Mt. Pinatubo (Thomason et al., 2018). Here we define large-magnitude eruptions as those with a Volcanic Explosivity Index (VEI; Newhall and Self, 1982) of 6 or more, and small-to-moderate-magnitude eruptions as those with a VEI of 3, 4, or 5 whereby we only consider those eruptions that had a measurable impact on the stratospheric aerosol load in the period 1979 to 2019 (see Table 1). The Mt.  
50 Pinatubo eruption was the largest stratospheric event since at least Krakatau in 1883 (Stothers, 1996). In the SAGE II record, the Mt. Pinatubo event remains clearly detectable until the late 1990s and thus it has an impact on nearly half of the 21-year dataset. In the seven years of SAGE II observations prior to Mt. Pinatubo, stratospheric aerosol levels consistently decrease following the 1982 El Chichón eruption (Thomason et al., 1997a). As a result, nearly 75% of the SAGE II record is dominated by the recovery from two large magnitude volcanic events. This can be clearly seen in Figure 1 where the long-term variation  
55 of stratospheric aerosol optical depth from the Global Space-based Stratospheric Aerosol Climatology (GloSSAC) is shown for 1979 through 2018 (Kovilakam et al., 2020). As a result, based on SAGE II observations, much of what is inferred as the ‘normal’ properties of stratospheric aerosol is skewed toward these large events rather than a handful of small-to-moderate events that occur throughout the period of interest.

As shown in Figure 1, starting with the January 2005 eruption of Manam, which is near the end of the SAGE II record, there  
60 are regular injections of aerosol and its precursors following volcanic eruptions. While none of these events approach the magnitude of Mt. Pinatubo or El Chichón, they were able to subtly modulate climate and are of general scientific interest (Solomon et al., 2011, Schmidt et al., 2018). From the end of the SAGE II mission in August 2005 until the start of the SAGE III/ISS mission in June 2017, space-based missions are mostly limited to single wavelength measurements associated with



instruments such as Optical Spectrograph and Infrared Imager System (OSIRIS, 2002- present) and Cloud-Aerosol Lidar with  
65 Orthogonal Polarization (CALIOP, 2006-present) (Rieger et al., 2019; Kar et al., 2019). Since the start of the SAGE III/ISS  
mission in June 2017, several additional small-to-moderate volcanic events have been observed including, Raikoke (June  
2019), Ulawun (June/August 2019), and two eruptions by Ambae in April and July 2018 (Kloss et al., 2020). In addition,  
there are at least two pyrocumulus<sup>1</sup> events, particularly the Canadian forest fire event of August 2017 (e.g., Bourassa et al.,  
2019) and the Australian bush fires of December 2019 and January 2020. The non-volcanic events are interesting but not the  
70 focus of this paper.

As shown in Figure 1, there is a significant qualitative difference in the stratospheric aerosol variability after the end of the  
SAGE II mission. It is also, until the start of the SAGE III mission, a period where the long-term stratospheric record is less  
robust due to the lack of global multiwavelength measurements of aerosol extinction coefficient. The initial impetus for this  
study was to develop tools to understand how reliably the long-term variability of stratospheric aerosol can be characterized  
75 given the limited data sets available. Thus, the original aim of this work was to understand how volcanic events manifest  
themselves in SAGE II/III observations with the goal of 1) inferring the uncertainty in single wavelength space-based data sets  
that use a fixed aerosol size distribution as a part of their retrieval algorithm such as the OSIRIS and CALIOP and 2) infer how  
well the wavelength dependence can be estimated for these single wavelength measurements. Both factors are relevant to long-  
term data sets constructed from diverse data sets such as GloSSAC (Kovilakam et al., 2020) as well as simply understanding  
80 the limitations in these data sets as standalone entities.

It should be clear from the outset that the solar occultation measurement strategy is, in general, not conducive to process studies  
and understanding the distribution of aerosol following highly localized events like volcanic eruptions. Following these sorts  
of events, we observe that SAGE observations have a high zonal variance in the data compared to more benign periods where  
the zonal variance is often not much larger than the measurement uncertainty particularly in the tropics (Thomason et al.,  
85 2010). The events we discuss below are not sampled in a temporally uniform way and the time between an eruption and the  
first SAGE II observations at the relevant latitudes varies from a few days to more than a month. This is an outcome of the  
sparse spatial sampling characteristic of solar occultation with latitudinal coverage dictation by orbital and seasonal  
considerations and a given latitude is measured at best once or twice per month. In addition, with 15 profiles per day with 24  
degrees of longitude spacing, the sampling is sparse in longitude even when latitudes of interest are available. Furthermore,  
90 aerosol properties in a single profile at a single altitude are the average of multiple samples along different line-of-sight paths  
through the atmosphere such that the spatial extent of a measurement at an altitude extends over hundreds if not thousands of  
square kilometers (Thomason et al., 2003). With these limitations, the ability to characterize the attributes of the early plume  
is limited.

The SAGE instruments use solar occultation to measure aerosol extinction coefficient at multiple wavelengths from the UV to  
95 the near infrared. These measurements are robust across a broad range of extinction levels and have a vertical resolution of

---

<sup>1</sup> Also called flammagenitus cloud



~1 km and are reported in 0.5 km increments from 0.5 to 40.0 km (Damadeo et al., 2013). The multi-wavelength aerosol extinction coefficient measurements provide limited information regarding the details of the aerosol size distribution of the aerosol (Thomason et al., 2008; Von Savigny and Hofmann, 2020) though many efforts at deriving the aerosol size distribution have been proposed (Yue and Deepak, 1983; Wang et al., 1996; Bingen et al., 2004; Malinina et al., 2018; Bauman et al., 2003; Anderson et al., 2000). The primary measure of particle size for SAGE II comes from the ratio of the aerosol extinction coefficient measurements at 525 and 1020 nm. Figure 2 shows the ratio for the Mie aerosol extinction coefficient for monodispersed aerosol (single radii). While a realistic size distribution complicates the picture, this relationship shows approximately how the inferred aerosol size changes with extinction coefficient ratio. Over the lifetime of the SAGE II mission, in the stratospheric aerosol layer, this ratio varies from around 5 (~0.2  $\mu\text{m}$ ) to values around 1 where the ability to discriminate aerosol is reduced to noting that the particles are ‘large’ with extinction dominated by aerosol larger than ~0.5  $\mu\text{m}$ . As shown in Figure 3, prior to the 1991 Mt. Pinatubo eruption, the stratospheric aerosol optical depth had a 525 to 1020-nm optical depth ratio of around 3.3 that changed with the first observations of the main Mt. Pinatubo cloud (in early July 1991) to a ratio of about 1.2 along with an a 525-nm optical depth increase by a factor of about 40. With low volcanic activity in this period, the relaxation of stratospheric aerosol loading toward background levels remains obvious in the tropics into the late 1990s. The Mt. Pinatubo event can lead to the perception that the ‘normal’ process is that volcanic input into the stratosphere generally increases aerosol extinction coefficient and decreases aerosol extinction coefficient ratio (suggesting an increase in the size of particles that dominate aerosol extinction). However, we will demonstrate below that the impact of volcanic events on stratospheric aerosol extinction coefficient ratio is strongly modulated by the magnitude of the eruption and, to a lesser extent, the stratospheric aerosol loading prior to the eruption. We will also show that the data suggests that sulfur rich but relatively ash-poor eruptions show a consistent, predictable behavior that lends itself as a test for interactive aerosol schemes used in global climate models. We also observe that the presence of large-size aerosol, probably ash, following a few eruptions significantly modulate these results.

### 3 Analysis

Herein, we examine the impact of 11 eruptions by 9 volcanoes (see Table 2) that affected the stratosphere for which there are SAGE II or SAGE III/ISS measurements available. Two volcanoes have two eruptions in this record: Ambae in April and July 2017 and Ulawun in June and August 2019. Due to SAGE III sampling the Ulawun events cannot be distinguished well and are treated as a single event. Overall, the eruptions increase aerosol extinction coefficient between  $10^{-4}$  and  $10^{-2}$   $\text{km}^{-1}$  relative to pre-eruption levels for a range of two orders of magnitude. These begin with the November 1985 eruption of Nevado del Ruiz (Colombia) and continue to the second eruption of Ulawun (Papua New Guinea) in August 2019 (see Table 2). From the associated observations, we infer the impact of these eruptions by noting the perturbation on the stratospheric aerosol extinction at both 525 and 1020 nm. The ratio of these perturbations provides a rough assessment of the impact of the eruptions on the size of particles dominating aerosol extinction. We analyze data from SAGE II and SAGE III/ISS in identical ways except for



one detail. The current version of SAGE III data (5.1) has a defect in which aerosol extinction at 521 nm is biased low below about 20 km due to an error in the O<sub>4</sub> absorption cross section used in processing this version. Since we wish to make the analysis coherent between instruments, we have replaced the 521 nm data product with an interpolation between 448 and 756 nm that employs a simple Angstrom coefficient scheme (602 nm and 676 nm measurements have biases like those at 521 nm). The differences between the inferred 521 nm extinction coefficients and the reported values in the lower stratosphere (tropopause to 25 km) are usually less than 10%.

For each event, we collect all SAGE II/III aerosol extinction coefficient data at 525 and 1020 nm between 10 and 25 km where the profiles occur within 10 deg of latitude of the eruption for a period starting 3 months prior to the eruption through 6 months following it. Depending on the latitude, as recorded in Table 2, and season, the volume and frequency of observations can vary significantly. Figure 4a shows all the data for Nevado del Ruiz in this temporal window at the altitude of the maximum increase in aerosol extinction coefficient, in this case 20.5 km. The Nevado del Ruiz eruption occurred on November 13 (Julian day 317) and the immediate enhancement of aerosol extinction coefficient is clear as aerosol extinction coefficient increases by about an order of magnitude from about 0.0007 km<sup>-1</sup> to values approaching 0.01 km<sup>-1</sup>. As shown in Figure 4b, the aerosol extinction coefficient ratio increases from about 2.2 prior to the eruption to a broad range of values from 2 to 3.5 in the immediately following the eruption (~day 380 or January 1986). The opposite of what was observed following the Mt. Pinatubo eruption as shown in Figure 3. The extinction ratio becomes much more consistent in the subsequent samples of this region of the stratosphere and falls from roughly 2.8 to 2.4 at the end of the analysis period (~day 560 or July 1986). The spread early in extinction coefficient and in extinction coefficient ratio is primarily due to inhomogeneity in the volcanic aerosol within the analysis area. This is suggested by Figure 5 in which the extinction coefficient ratio is plotted versus the extinction coefficient for this data set. Almost without exception, the enhancement in aerosol extinction coefficient is associated with larger values of extinction coefficient ratio. The distinction between volcanically perturbed observations and the unperturbed periods prior to the eruption is clearly recognizable. A handful of points show very high aerosol extinction coefficient and low extinction coefficient ratio. It is possible that these are observations of volcanic ash possibly mixed with the sulfuric acid aerosol. In any case, these points are rare and only occur in the first month following the eruption. Generally, we find that the low latitude eruptions have lower variance in aerosol extinction coefficient than mid and high latitude events. This was particularly apparent in the SAGE III/ISS observations of the Canadian pyrocumulus event of August 2017 (Bourassa et al., 2019) where some profiles in northern mid latitudes showed perturbations as large as 10<sup>-2</sup> km<sup>-1</sup> whereas other profiles in the same latitude band showed no perturbation at all throughout September and October 2017. In this regard, the lower variance, low latitude events are a more straightforward evaluation than high variance, higher latitude events.

Given the geometry of the solar occultation measurements, SAGE II and III sample a latitude band episodically, revisiting a latitude every few weeks to months. This sampling pattern is clear in Figure 4a and 4b. We make use of this pattern and average the extinction values at both 525 and 1020 nm into these irregularly spaced and duration bins. In this averaging process, we select the maximum values of extinction coefficient at 1020 nm from each profile within a 9-point window from 1 km below to 3 km above it around the broadly observed maximum in the extinction profiles (20.5 km in this case) as we try to



capture the behavior of the main aerosol layer (as opposed to the entire layer) of the eruption including a tendency for the layer to increase in altitude during the months following the eruption. For events in this analysis, there is a 0.5 to 2 km rise in the altitude of peak aerosol extinction during the analysis period following the eruption due mostly to dynamical processes (Vernier et al., 2011). To produce a mean value, we required a minimum of 6 points which eliminates a few periods such as the few points around Julian day 340 and again around Julian day 350 as seen in Figure 4a. The averaging then produces a simplified characterization of the effects of the eruption as shown in Figure 6. In this figure, we see that the change in aerosol extinction coefficient (solid) and extinction coefficient ratio (dash) are well correlated with both reaching a maximum near Julian day 380 (as sampled by SAGE II). One difference is that while both parameters begin to relax back toward pre-eruptive levels, the extinction coefficient does so quite a bit more quickly than the extinction coefficient ratio. Since the scale for the extinction coefficient ratio does not extend to zero, the difference in the recovery rates is even more significant. Figure 7 shows the same plots for the remaining nine eruptions. They can be crudely sorted into a few categories. Several show similar characteristics as the Nevado del Ruiz eruption with a rapid increase in aerosol extinction coefficient and ratio following an eruption. These tend to be among the smaller eruptions and include: Cerro Hudson in 1991 (Figure 7c), Manam in 2005 (Figure 7e), Ambae twice in 2018 (Figure 7f), and Ulawun twice in 2019 (Figure 7g). Several volcanic events show the opposite behavior with a decrease in extinction ratio following an event including Mt. Pinatubo in 1991 (Figure 7b) and Raikoke in 2019 (Figure 7g). A few seem to follow their own unique paths: Kelut in 1990 (Figure 7a) and Ruang in 2002 (Figure 7d). We will discuss some of these events in more detail below.

Figure 8a shows the before-and-after state of the main aerosol layer for these 10 eruptions where ‘before’ or the baseline values are defined as the first data point in the series and the ‘after’ is defined where the 1020 nm aerosol extinction coefficient reaches a maximum. As one could infer from Figure 7, we see two types of events, those with positive slopes (larger extinction/larger extinction ratio) and those with negative slopes (larger extinction/smaller extinction ratio) with some suggestion of a change of slope from strongly positive to negative with increasing extinction coefficient perturbation. To isolate this change, we define an aerosol extinction coefficient perturbation to be

$$\delta k_{\lambda} = k_{\lambda}(\text{max}) - k_{\lambda}(\text{baseline})$$

which is computed for 1020 and 525 nm where 1020 nm aerosol extinction coefficient is a maximum. It should be noted that the maximum extinction coefficient at 525 nm does not necessarily occur at the same altitude or time as the maximum in 1020 nm extinction coefficient. We define a perturbation aerosol extinction coefficient ratio as

$$\text{ratio} = \delta k_{525} / \delta k_{1020}.$$

Figure 8b shows the relationship between the *perturbation* parameters. There is a reasonably well-behaved relationship for 8 of these events with a straight line or modest curve from the smallest perturbation event (Manam) and the largest (Mt. Pinatubo). At some point we would expect that the relationship would asymptote to about 1 for large events near or larger than Mt. Pinatubo, reflecting the presence of very large radius aerosol (>0.4 μm) so some sort of curvature seems reasonable. While the perturbation ratio approach effectively treats the aerosol as an add-on to the baseline aerosol extinction, we do not suggest that volcanic aerosol does not interact with the pre-existing aerosol. Nonetheless, the observed relationship in Figure 8b



suggests that the values of the perturbation pair (extinction coefficient and extinction ratio) are insensitive to the initial conditions of the stratospheric aerosol. This relationship suggests a potential route to inferring uncertainty in the OSIRIS and CALIOP data during the SAGE II to SAGE III/ISS gap period by estimating changes in the extinction coefficient slope (or Angstrom coefficient) based on perturbations in those instruments' measured quantities. It also suggests a potential use in  
200 evaluating interactive aerosol modules for GCMs and ESMs for a broad range of volcanic events including ones not explicitly observed by space-based instruments.

Despite the close timing of the two Ambae eruptions in 2018 eruptions (April and July), the eruptions are clearly distinguishable in the SAGE III/ISS data shown in Figure 7f with the later eruption many times more intense than the earlier one. Individually, the Ambae (Vanuatu) eruptions in 2018 are similar to the Nevado del Ruiz eruption discussed in detail above  
205 as both show an increase in the extinction coefficient and extinction coefficient ratio relative to the values seen in early 2018 that is characteristic of most small-to-moderate eruptions. However, the extinction coefficient ratio decreases following the second eruption suggesting that the second eruption may be an outlier to the generally observed behavior. To calculate the perturbations for these two events we use data from prior to the first eruption as the baseline for both though the results for the second eruption are insensitive to the perturbation caused by the earlier eruption. The initial Ambae eruption increased the  
210 extinction coefficient ratio from 3.2 to nearly 5 with an increase of 1020 nm extinction from about  $1e-4$  to about  $3e-4$ . The second eruption decreased the ratio from 4.9 to 4.1 with an extinction increase of  $2.e-4$  to  $1.3e-3$  or about a factor of 6 (Figure 7f). With these values, and despite appearances, both eruptions fit well with the majority of the other events shown in Figure 8b. In this case, the eruptions occur at slightly different altitudes so the apparent rise in the aerosol layer from the beginning to the end of the period is a little larger than for most events ( $\sim 2$  km). In this case, particularly for the second eruption, the  
215 extinction change is so large that the impact of the pre-eruption aerosol values is negligible. Another interesting feature is that the largest ratios after the eruption do not necessarily coincide with the largest extinction. Figure 9 shows the extinction latitude/altitude cross sections for September 2018 for 521 nm (Figure 9a), 1020 nm (Figure 9b) and their ratio (Figure 9c). It is clear here that the maximum in the extinction ratio lies below the main peak in extinction coefficient in the tropics and, notably stretches to higher southern latitudes and the maximum values actually occurs near  $30^\circ$  S despite more inhomogeneous conditions at this latitude than in the tropics. This is not an obvious outcome, but it is consistent with the general observation  
220 that the largest perturbations in extinction ratio occur with smaller extinction coefficient perturbations as shown in Figure 8b. It also shows the importance of keeping in mind that the relationship between extinction coefficient perturbation and overall extinction ratio in Figure 8b is for the main aerosol layer and not all parts of the volcanic cloud. That the dependence of aerosol extinction coefficient perturbation ratio on extinction coefficient perturbation occurs within a particular eruption as well as  
225 among different eruptions (for the peak values shown in Figure 8) implies that a consistent physical process is at work.

There are two events lying considerably away from Figure 8b's main curve: Kelut (1990) and Ruang. For Kelut, the first observations take place about 10 days after the eruption. This is where the ratio is the lowest (Figure 7a) and it increases from 2.2 to 2.6 in following few weeks and then to 3.0 at the end of the observation period. Ruang shows some similar features with the low perturbation extinction ratio (2.7) occurring shortly after the eruption followed by a recovery toward larger values



230 in the weeks that follow (4.3). The Kelut scatter plot (Figure 10) shows that while the extinction coefficient and ratio are compact for most of this period, there are some observations of higher extinction and ratios approaching one which occur in the earliest observation period suggesting the immediate presence of large aerosol ( $>0.5 \mu\text{m}$ ). While the data itself does not provide certainty, it is possible that an extinction-dominating presence of ash particles rather than sulfuric acid particles in the main aerosol layer immediately after the eruption may push its perturbation location below the rough curve suggested by most  
235 of the events. Similar data from Ruang is less illuminating due to a much smaller sample of data in the 50% duty cycle period of SAGE II data (after the end of 2000) and it is not possible to infer a cause for its anomalous position in Figure 8b. Both eruptions show increased aerosol extinction coefficient ratios away from the main aerosol peak suggesting, at least in part, behavior more consistent with most eruptions.

Another interesting feature is the spread among the Nevado del Ruiz, Cerro Hudson and Raikoke eruptions which cause very  
240 similar extinction coefficient perturbations but different perturbation extinction ratios. The position of Nevado del Ruiz in Figure 8b is consistent with the overall perturbation relationship. Raikoke lies on the same side as the Kelut and Ruang eruptions but, unlike Kelut, there is little evidence of large extinction/small extinction ratio observations (possible ash) at the peak extinction level as essentially all the data follows the mean relationship in Figure 7g. Since Raikoke is one of only two mid latitude eruptions in the data set, it is possible that latitude plays a role in the perturbation relationship. However, Cerro  
245 Hudson lies closer to Nevado del Ruiz's position in Figure 8b and is a similar event to Raikoke as it occurs at a similar latitude and season and at a similar pre-eruption aerosol extinction coefficient level. It is possible that atmospheric conditions or some detail of eruptions can have a modulating impact on how events manifest themselves in extinction coefficient and ratio but not be easily detectable from the data alone. For instance, for Raikoke, we cannot exclude the possibility of the presence of small amounts of ash embedded in the main aerosol layer with the sulfuric acid aerosol influencing the extinction coefficient and  
250 ratio. It is also possible that a pyrocumulus event, that occurred in Alberta, Canada just prior to the Raikoke eruption, plays a role in the evolution of extinction following this event. To some extent, while we are fortunate to have as many events for this analysis as we do, it is still a relatively small sample and some factors that can impact the extinction coefficient/ratio relationship may not be fully revealed.

#### 4 Discussion

255 Without a detailed simulation of the aerosol microphysical processes at play we can speculate that small-to-moderate eruptions are initially dominated by small ( $\sim 1 \text{ nm}$ ), mostly homogeneously nucleated particles that are present in very large number densities. These are initially invisible to the extinction measurements (as shown in Figure 11) but coagulate into steadily larger particles (possibly consuming small-sized aerosol present in the pre-existing aerosol layer) that produce perturbations to the observed aerosol extinction and ratio that reflect their magnitude as shown in Figure 8b. This process generally causes an  
260 increase in aerosol extinction coefficient ratio but may produce the opposite effect depending on the properties of the aerosol present prior to the eruption. The coagulation process continues producing ever larger aerosol and smaller particle number





densities until coagulation is no longer efficient at the times scales we examine here and with respect to mixing of the material within the stratosphere. For large magnitude eruptions, like Mt. Pinatubo, it is possible that volcanic precursor gases and vapors primarily condense onto existing aerosol and/or these and very small, homogeneously nucleated aerosol particles more rapidly coagulate to form larger-sized aerosol and, thus, the aerosol extinction coefficient ratio decreases as shown in Figure 8a.

We have modelled volcanic aerosol perturbation using a simple model in which we determine the volume density of aerosol required to produce 1020-nm extinction coefficient perturbations of  $10^{-4}$ ,  $10^{-3}$ , and  $10^{-2} \text{ km}^{-1}$  at a single-radius of 500 nm. This can be expressed using

$$n(r) = \frac{\delta k_{\lambda}}{Q_{\lambda}(r)\pi r^2}$$

and

$$V = \frac{4\pi r^3 n(r)}{3}$$

where  $\delta k_{\lambda}$  is the extinction coefficient perturbation at wavelength  $\lambda$  (in this case 1020 nm),  $r$  is particle radius (500 nm),  $n(r)$  is the inferred particle number density,  $Q_{\lambda}(r)$  is the Mie scattering efficiency for the wavelength and radius considered for sulfuric acid aerosol at stratospheric temperatures, and  $V$  is the required volume density of aerosol. The choice of 500 nm for this calculation is somewhat arbitrary and any value would not affect the conclusions drawn from this study. For an extinction perturbation of  $10^{-2} \text{ km}^{-1}$  the number density is  $4.50 \text{ cm}^{-3}$  with a volume density of  $2.37 \mu\text{m}^3/\text{cm}^3$ . Holding  $V$  fixed, we compute number density and the aerosol extinction coefficient perturbation as a function of radius at 525 and 1020 nm using

$$n(r) = 3V/4\pi r^3$$

and

$$\delta k_{\lambda} = Q_{\lambda}(r)n(r)\pi r^2$$

for radii,  $r$ , from 1 to 500 nm. The ratio of these perturbations follows the relationship shown in Figure 2. Finally, we add baseline aerosol extinction coefficient values we previously determined for the Nevado del Ruiz eruption and the July 2018 Ambae eruption and show these relationships in Figure 11a and 11b respectively. Due to their different pre-eruption extinction levels, the extinction ratio plots shown for the two volcanic events are notably different despite having identical perturbations. This is consistent with the data shown in Figure 8a. To some extent, the radius axis in this plot is akin to a time axis though a particularly non-linear one. It is likely that the transition across the smallest size particles is extremely rapid (relative to SAGE-like observation timescales at least) and the large end of the timescale may effectively be reached rapidly for large events like Mt. Pinatubo but effectively never for small-to moderate eruptions due to the other processes that control coagulation and other aspects of aerosol morphology. Indeed, the first observations of the main Mt. Pinatubo cloud in early July 1991, a few weeks after the eruption, show an extinction coefficient ratio of essentially 1. Whether this would have been the case with observations immediately after the eruption is an interesting unknown.



If the initial growth to 200 nm is rapid at SAGE temporal sampling scales (~monthly), the model simulations qualitatively reproduce the increase in extinction coefficient ratio seen in many of the eruptions analyzed with a step increase in extinction coefficient ratio followed by a decrease in time. In addition, these results show that, while the perturbations themselves may be insensitive to the baseline stratospheric state, the result is not. In fact, scenarios can be easily constructed in which the same eruption, again with minimal interaction with the pre-existing aerosol, results in a different sign in the slope of the change in extinction coefficient ratio. A less obvious outcome of this modelling is that the relationship between extinction ratio and effective radius, which is frequently treated as invariant, is likely far different in the aftermath of a volcanic eruption than in more quiescent periods. Obviously, we must exercise caution in interpreting the observations based on the simple model employed here. For instance, since we do not know the timescale of coagulation, significant uncertainty remains in how to interpret Figure 8b in a temporal sense. Moreover, aerosol volume density is unlikely to be constant over this time is a significant assumption as the conversion of SO<sub>2</sub> to H<sub>2</sub>SO<sub>4</sub> has a time constant on the order of 30 days and depends on the magnitude of the eruption. Nonetheless, while not a primary goal for this study, we believe this very simple model suggests that SAGE II/III observations are consistent with volcanic material primarily condensing homogeneously followed by coagulation whose timescale depend on the magnitude of the eruption.

## 5 Conclusions

Herein, we have used SAGE II/III observations to examine the behavior of stratospheric aerosol extinction coefficient in the aftermath of small-to-large magnitude volcanic events. We have focused on the initial plume development at the peak extinction levels and not the long-term development or the details of its distribution as transport and other aerosol processes such as sedimentation have not been considered. We have found that SAGE observations of the peak perturbations in stratospheric aerosol extinction levels following volcanic eruptions show, under most circumstances, a crude independence to the characteristics of the pre-existing aerosol and that these perturbations follow a predictable behavior. While this relationship is insensitive to the pre-existing aerosol, the pre-existing aerosol can modulate the observed changes in extinction ratio. The analysis is straightforward for tropical eruptions but more challenging for mid and high latitude eruptions where transport is generally more complex than in the tropics. Also, it is possible that volcanic events with significant amounts of ash may behave considerably different than those dominated by the sulfuric acid component.

The perturbation relationship is based only on the measurements themselves and makes no assumptions about the underlying composition or size distribution of the aerosol. In this respect, it is a unique tool to verify that interactive aerosol models used in GCMs and ESMs reproduce the observed behavior. This should be extremely straightforward as extinction coefficient can be calculated from aerosol products already produced by these modules though care would need to be exercised to reproduce the measurement paradigms used herein. Since the results span a large dynamic range of aerosol extinction coefficient perturbations (> two orders of magnitude), the testing range covers a significant range of volcanic events. Since the observed



325 relationship is well behaved, testing is potentially not limited to observed volcanic events but may be applied to hypothetical events or historical events for which space-based observations do not exist.

The primary goal of this effort was to assess data quality of data sets consisting of a single wavelength measurement of aerosol extinction coefficient or similar parameter particularly when a fixed aerosol size distribution is a part of the retrieval process. This is important as a part of the data quality assessment of these data sets as well as their use in long-term data sets such as  
330 GloSSAC. In this regard, the results are mixed. It is clear from Figure 8b that the wavelength dependence of a predominating sulfuric acid volcanic event can be estimated from the relationship shown therein. Since a fixed particle size distribution is used in the OSIRIS retrieval process, a fixed wavelength dependence is effectively intrinsic to the OSIRIS aerosol extinction coefficient retrieval process. As a result, it is not immediately clear how to incorporate an estimate for the wavelength dependence of aerosol extinction coefficient from this work into the OSIRIS process. We believe that we may be able to use  
335 these results in spot applications such as assessing the extinction error due to the fixed aerosol size distribution in the immediate aftermath of an event however a general correction for the entire record requires further consideration.

#### **Code and data availability.**

SAGE II ([https://doi.org/10.5067/ERBS/SAGEII/SOLAR\\_BINARY\\_L2-V7.0](https://doi.org/10.5067/ERBS/SAGEII/SOLAR_BINARY_L2-V7.0)) and SAGE III/ISS data ([https://doi.org/10.5067/ISS/SAGEIII/SOLAR\\_HDF4\\_L2-V5.1](https://doi.org/10.5067/ISS/SAGEIII/SOLAR_HDF4_L2-V5.1)) are accessible at the NASA Atmospheric Sciences Data  
340 Center. GloSSAC v2.0 (<http://doi.org/10.5067/GLOSSAC-L3-V2.0>) is available from the same location. Data analysis products shown herein are available from the corresponding author.

#### **Author contributions.**

LWT developed the analysis tools used throughout the paper and was the primary of author of the manuscript. MK and LR advised the author particularly in relationship to the GloSSAC data set and issues related to OSIRIS data quality and  
345 algorithms. AS suggested the conceptual model used to characterize the way small-to-moderate volcanic eruptions affect aerosol extinction ratio. CvS and TNK advised regarding the use and modeling of the SAGE data sets. Finally, all authors provided substantial input on the construction of the manuscript and figures.

#### **Competing interests.**

The authors declare that they have no conflict of interest.

#### **350 Acknowledgements.**

We acknowledge the support of NASA Science Mission Directorate and the SAGE III/ISS mission team.



### **Financial support.**

LWT, MK and TNK are supported by NASA's Earth Science Division as a part of the ongoing development, production, assessment, and analysis of SAGE data sets. Stratospheric aerosol research at the University of Greifswald (CvS) is funded by 355 DFG (project VolARC of the DFG Research Unit VolImpact, FOR 2820; grant number 398006378). AS received funding from UK Natural Environment Research Council (NERC) grants NE/S000887/1 (Vol-Clim) and NE/S00436X/1 (V-PLUS). Work performed by LR was funded by the Canadian Space Agency under the Earth Science System Data Analyses program.



360 **Table 1. Volcanic eruptions and smoke events that significantly impact stratospheric aerosol levels in the Version 2.0 of the GloSSAC data set (Kovilakam et al., 2020) and denoted in Figure 1 using the abbreviation in brackets following the name.**

<b>Volcano Name</b>	<b>Eruption Date</b>	<b>Latitude</b>
<i>St. Helens (He)</i>	27 Mar 1980	46° N
<i>El Chichon (El)</i>	4 Apr 1982	17° N
<i>Nevado del Ruiz (Ne)</i>	14 Nov 1985	5° S
<i>Kelut (Ke)</i>	10 Feb 1990	8° S
<i>Pinatubo (Pi)</i>	15 Jun 1991	15° N
<i>Cerro Hudson (Ce)</i>	12 Aug 1991	46° S
<i>Rabaul (Ra)</i>	19 Sept 1994	4° S
<i>Ulawun (Ul)</i>	29 Sept 2000	5° S
<i>Shiveluch (Sh)</i>	22 May 2001	56° N
<i>Ruang (Rn)</i>	25 Sept 2002	2° N
<i>Reventador (Rv)</i>	03 Nov 2002	0° N
<i>Manam (Mn)</i>	27 Jan 2005	4° S
<i>Soufriere Hills (Sh)</i>	20 May 2006	16° N
<i>Tavurvur (Tv)</i>	07 Oct 2006	4° S
<i>Chaiten (Ch)</i>	02 May 2008	42° S
<i>Okmok (Ok)</i>	12 Jul 2008	55° N
<i>Kasatochi (Ka)</i>	07 Aug 2008	55° N
<i>Fire/Victoria (Vi)</i>	07 Feb 2009	37° S
<i>Sarychev (Sv)</i>	12 Jun 2009	48° N
<i>Nabro (Nb)</i>	13 Jun 2011	13° N
<i>Kelut (Ke)</i>	13 Feb 2014	8° S
<i>Calbuco (Cb)</i>	22 April 2015	41° S
<i>Canadian Wildfires (Cw)</i>	August 2018	51° N
<i>Ambae (Am)</i>	27 July 2018	15° S



365 **Table 2. Volcanic events observable in the SAGE II (1984-2005) and SAGE III/ISS (2017-present) records including the total number of observations used in the analysis.**

<i>Eruption</i>	<i>Date</i>	<i>Latitude</i>	<i>Altitude (km)</i>	<i>SAGE Observations</i>
<i>Nevado del Ruiz</i>	13 November 1985	5° N	20.5	634
<i>Kelut</i>	10 February 1990	8° S	20.5	523
<i>Mt. Pinatubo</i>	17 June 1991	15° N	22.0	433
<i>Cerro Hudson</i>	8 August 1991	46° S	11.5	1162
<i>Ruang</i>	25 September 2002	9° S	18.5	255
<i>Manam</i>	27 January 2005	4° S	20.0	219
<i>Ambae</i>	5-6 April 2018/28 July 2018	15° S	18.0	858
<i>Raikoke</i>	22 June 2019	48° N	15.0	1014
<i>Ulawun</i>	26 June 2019/3 August 2019	5° S	18.5	491

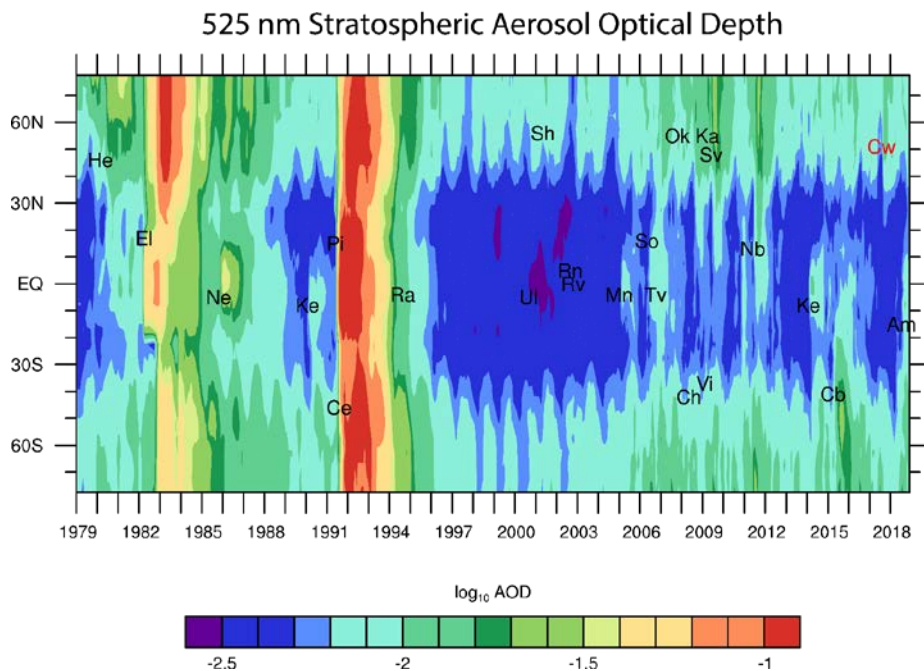


**Figure 1.** Stratospheric aerosol optical depth at 525 nm from GloSSAC v2.0 [Kovilakam et al., 2020]. Volcanic and similar events are denoted using abbreviations given in Table 1.

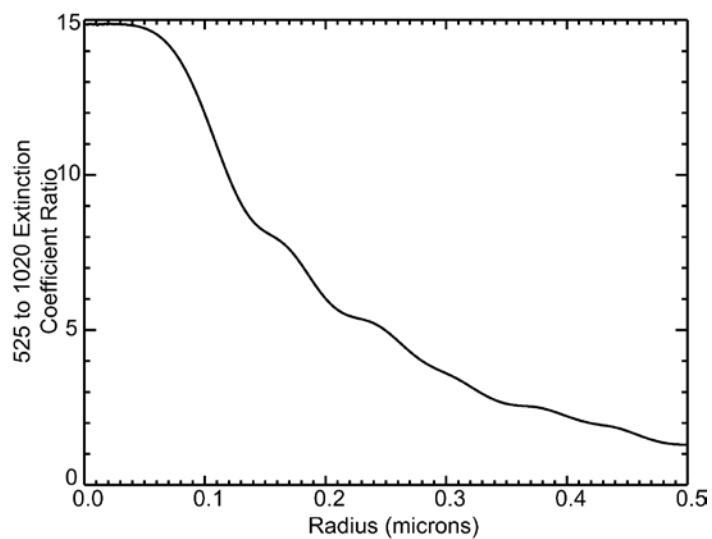


**Figure 2.** The ratio of extinction coefficient at 525 to 1020 nm for single particles as a function of radius for sulfuric acid aerosol at stratospheric temperatures.





370

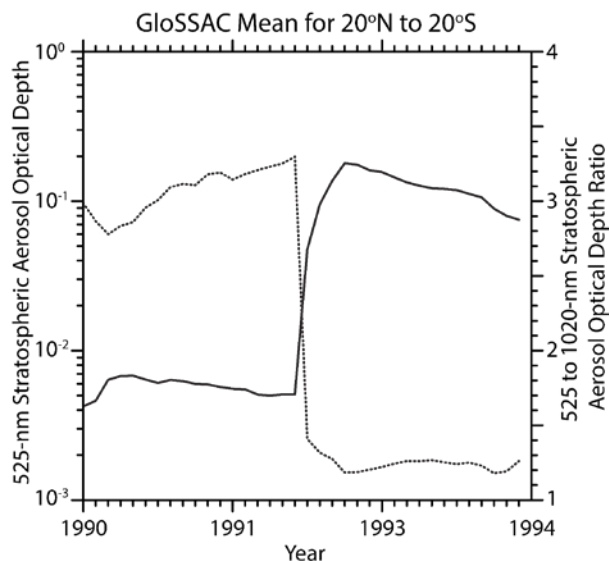


**Figure 3.** The GloSSAC depiction of 525-nm aerosol optical depth (solid) and 525 to 1020-nm stratospheric aerosol optical depth ratio (dotted) for 1990 through the end of 1993 encompassing the Kelut eruption in early 1990 and the Mt. Pinatubo eruption in mid-1991.

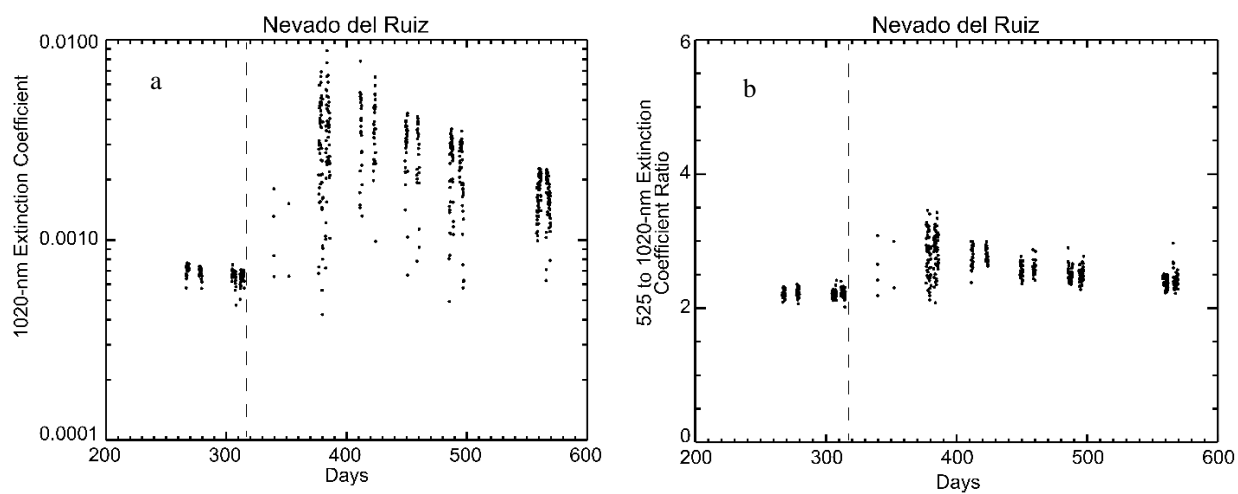


**Figure 4.** The scatter of SAGE II 1020-nm aerosol extinction coefficient in  $\text{km}^{-1}$  (a) and 525 to 1020-nm aerosol extinction coefficient ratio (b) at 20.5 km between 10S and 10N in days from 1 January 1985.

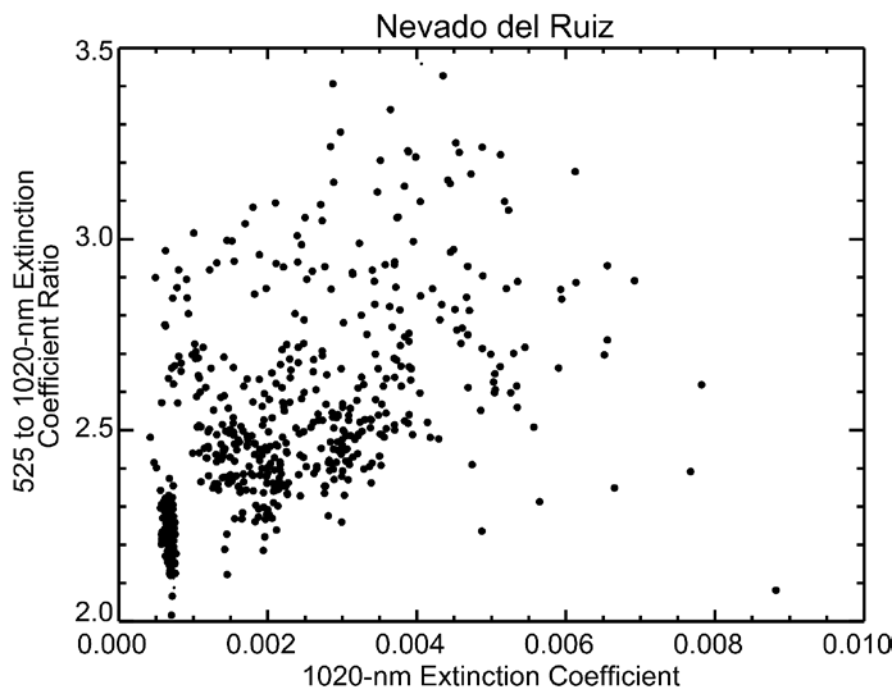


**Figure 5.** Same data as shown in Figure 3 except now plotted as 1020-nm aerosol extinction coefficient (in  $\text{km}^{-1}$ ) versus the extinction coefficient ratio. The extinction coefficient ratio is a rough estimate of the size of aerosol particles that dominate extinction. Values near 1 suggest particle radius greater than  $\sim 0.4 \mu\text{m}$  with increasing value indicating smaller particles.

380

385



390

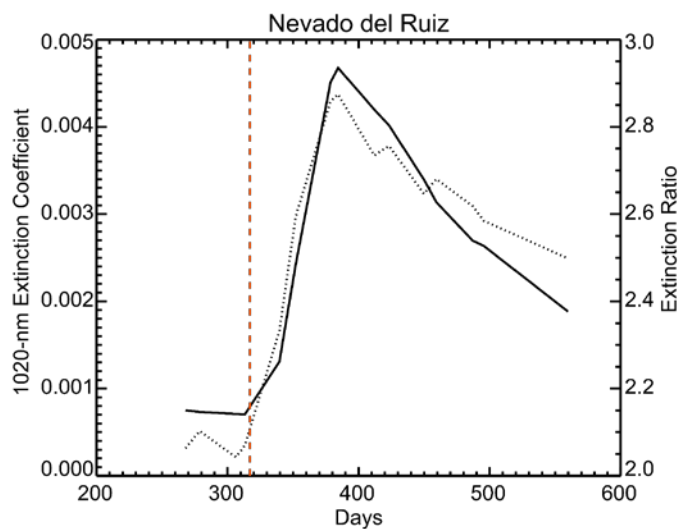


**Figure 6.** Same data as shown in Figure 4 except averaged in temporal data clusters. In this figure, extinction coefficient is the solid line and the extinction coefficient ratio is the dotted line. The date of the eruption is denoted by the vertical dashed line.

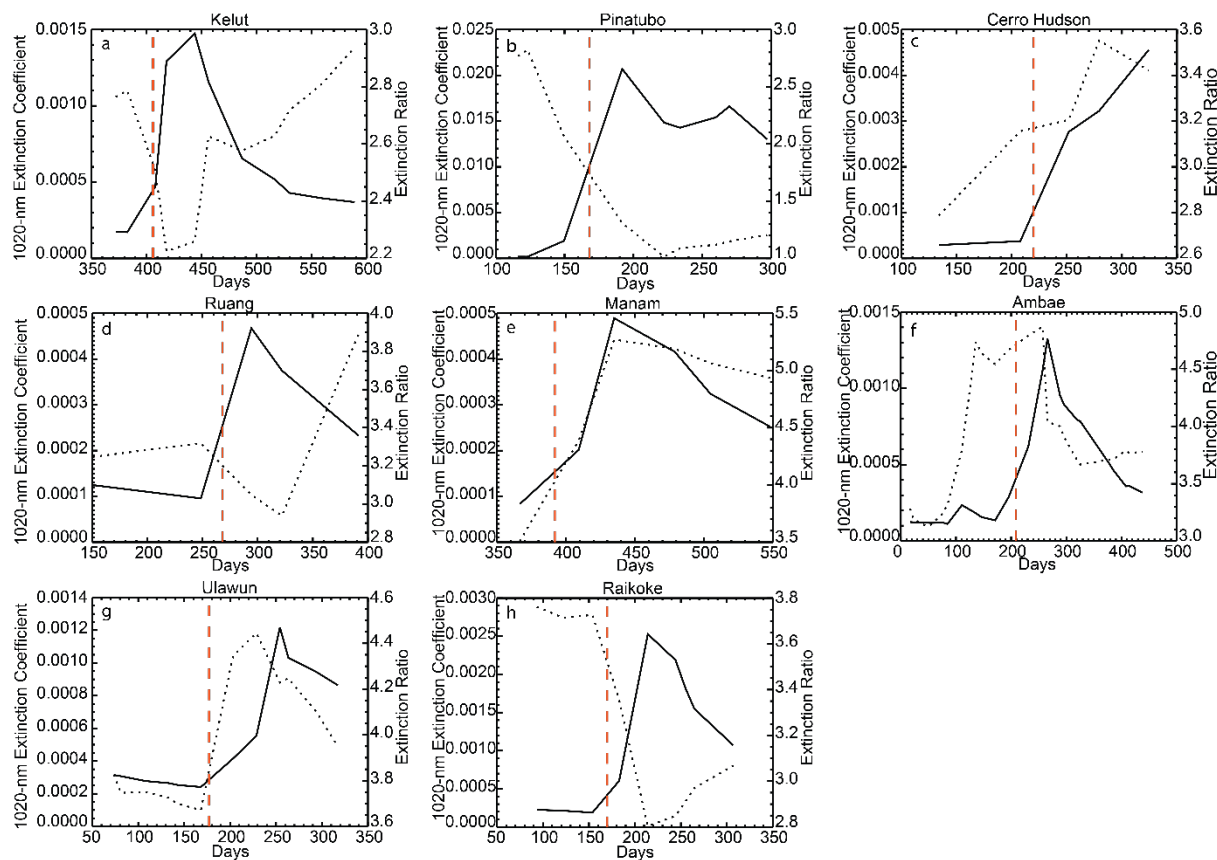


**Figure 7.** Similar analysis as shown in Figure 6 except for Kelut in 1990 (a), Mt. Pinatubo (b) and Cerro Hudson (c) in 1991, Ruang in 2002 (d), Manam in 2005 (e), Ambae in 2018 (f), Ulawun (g) and Raikoke (h) in 2019. In each frame, extinction coefficient is the solid line and the extinction coefficient ratio is the dotted line. The date of the eruption is denoted by the vertical dashed line.

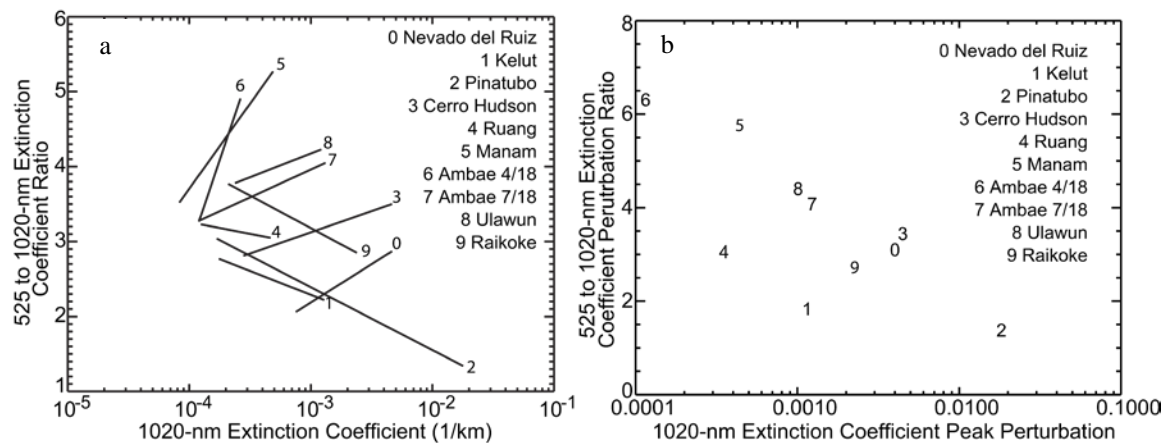
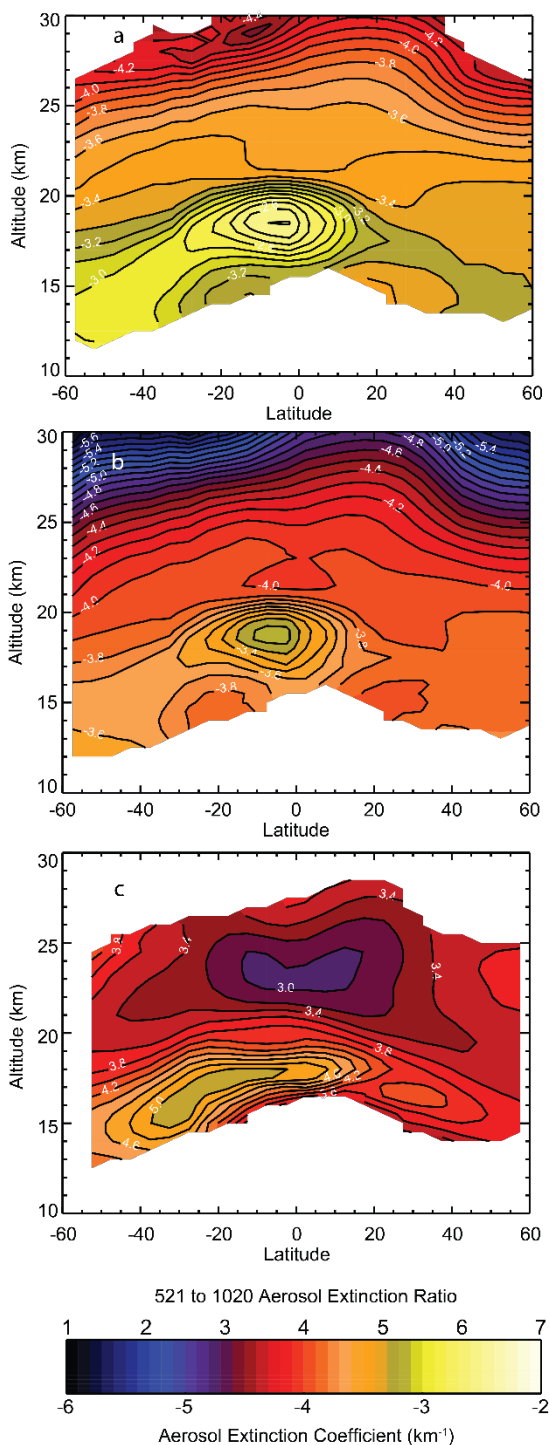


**Figure 8.** The baseline (before) to peak 1020-nm aerosol extinction coefficient for the 10 eruptions considered in this study is shown in frame (a) with the differences between them (perturbations) are shown in frame (b).

400

405



410 **Figure 9.** Mean SAGE III/ISS 525 (a) and 1020 nm (b) aerosol extinction coefficient and 525 to 1020-nm aerosol extinction coefficient ratio (c) as a function of latitude and altitude from August 2019 shortly after the second 2018 eruption of Ambae (July 2018).

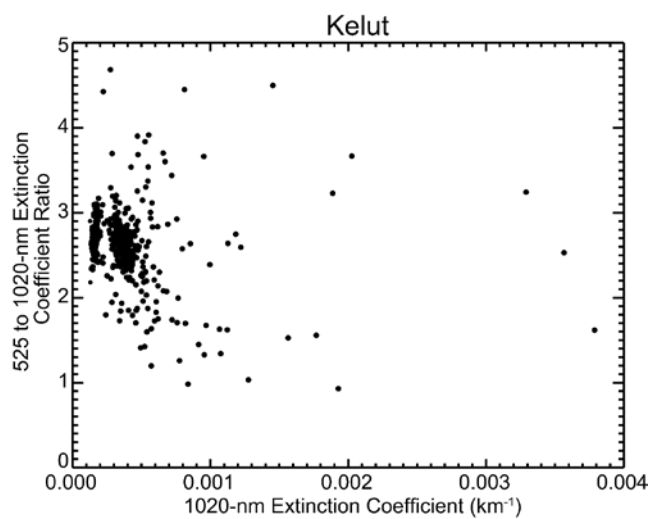


**Figure 10.** SAGE II 525 to 1020 nm aerosol extinction coefficient ratio plotted versus 1020-nm aerosol extinction coefficient in  $\text{km}^{-1}$  during the Kelut event from December 1989 through August 1990 plotted at 20.5 km between 20S and the Equator.



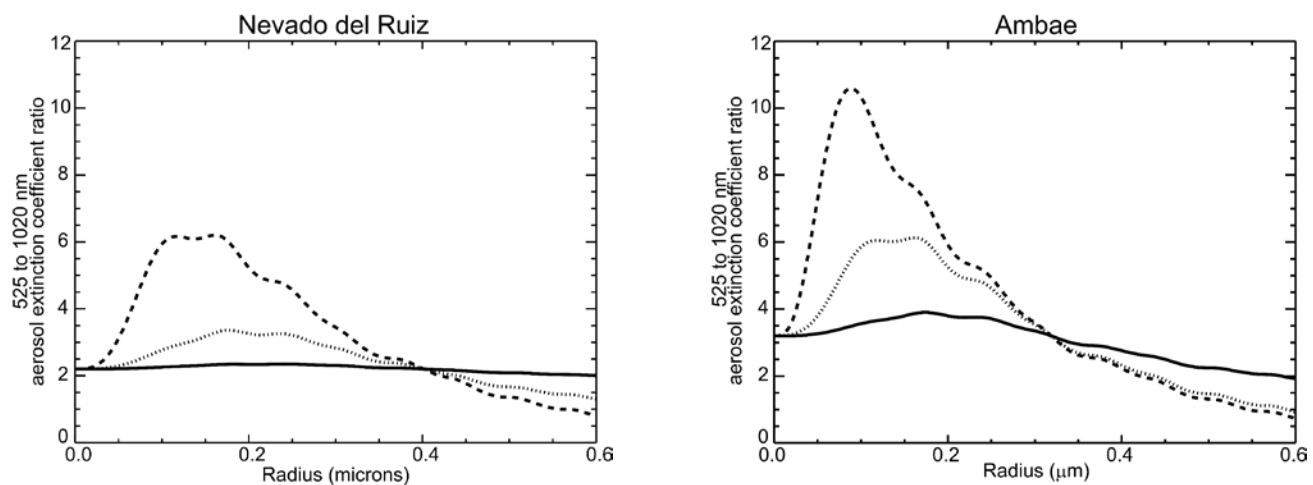


**Figure 11.** Estimated 525 to 1020-nm aerosol extinction ratio for fixed aerosol volume density perturbations and single-radii particles that yield a perturbation at 500 nm of  $10^{-4}$  (solid),  $10^{-3}$  (dotted), and  $10^{-2}$  km<sup>-1</sup> (dashed) using baseline 525 and 1020 nm extinction coefficient values for Nevado del Ruiz (a) and Ambae (b).



## 415 **References**

- Anderson, J., Brogniez, C., Cazier, L., Saxena, V. K., Lenoble, J., and McCormick, M. P.: Characterization of aerosols from simulated SAGE III measurements applying two retrieval techniques, *Journal of Geophysical Research-Atmospheres*, 105, 2013-2027, doi.org/10.1029/1999jd901120, 2000.
- Bauman, J. J., Russell, P. B., Geller, M. A., and Hamill, P.: A stratospheric aerosol climatology from SAGE II and CLAES  
420 measurements: 1. Methodology, *Journal of Geophysical Research-Atmospheres*, 108, doi.org/10.1029/2002jd002992, 2003.
- Bingen, C., Fussen, D., and Vanhellemont, F.: A global climatology of stratospheric aerosol size distribution parameters derived from SAGE II data over the period 1984-2000: 1. Methodology and climatological observations, *Journal of Geophysical Research-Atmospheres*, 109, doi.org/10.1029/2003jd003518, 2004.
- Bourassa, A., Rieger, L., Zawada, D. J., Khaykin, S., Thomason, L., and Degenstein, D.: Satellite limb observations of  
425 unprecedented forest fire aerosol in the stratosphere, *J. Geophys. Res.*, 124, 9510-9519, doi.org/10.1029/2019JD030607, 2019.
- Chu, W. P., and McCormick, M. P.: Inversion of stratospheric aerosol and gaseous constituents from spacecraft solar extinction data in the 0.38-1.0-mm wavelength region, *Applied Optics*, 18, 1404-1413, 1979.
- Damadeo, R. P., Zawodny, J. M., Thomason, L. W., and Iyer, N.: SAGE version 7.0 algorithm: application to SAGE II,  
430 *Atmospheric Measurement Techniques*, 6, 3539-3561, doi.org/10.5194/amt-6-3539-2013, 2013.
- Kar, J., Lee, K. P., Vaughan, M. A., Tackett, J. L., Trepte, C., Winker, D., Lucker, P., and Getzewich, B.: CALIPSO level 3 stratospheric aerosol profile product: version 1.00 algorithm description and initial assessment, *Atmos Meas Tech*, 12, 6173-6191, doi.org//10.5194/amt-12-6173-2019, 2019.
- Kloss, C., Sellitto, P., Legras, B., Vernier, J.-P., Jegou, F. R., Ratnam, M. V., Kumar, B. S., Madhavan, B. L., and Berthet, G.:  
435 Impact of the 2018 Ambae eruptions on the global stratospheric aerosol layer and climate, *J. Geophys. Res.*, doi.org//10.1002/essoar.10501617.1, 2020.
- Kovilakam, M., Thomason, L., Ernest, N., Rieger, L., Bourassa, A., and Millán, L.: The Global Space-based Stratospheric Aerosol Climatology v2.0, *Earth System Science Data*, 2020.
- Kremser, S., Thomason, L. W., von Hobe, M., Hermann, M., Deshler, T., Timmreck, C., Toohey, M., Stenke, A., Schwarz, J.  
440 P., Weigel, R., Fueglistaler, S., Prata, F. J., Vernier, J. P., Schlager, H., Barnes, J. E., Antuña-Marrero, J. C., Fairlie, D., Palm, M., Mahieu, E., Notholt, J., Rex, M., Bingen, C., Vanhellemont, F., Bourassa, A., Plane, J. M. C., Klocke, D., Carn, S. A.,



- Clarisse, L., Trickl, T., Neely, R., James, A. D., Rieger, L., Wilson, J. C., and Meland, B.: Stratospheric aerosol-Observations, processes, and impact on climate, *Reviews of Geophysics*, 54, 278-335, doi.org/10.1002/2015rg000511, 2016.
- Malinina, E., Rozanov, A., Rozanov, V., Liebing, P., Bovensmann, H., and Burrows, J. P.: Aerosol particle size distribution  
445 in the stratosphere retrieved from SCIAMACHY limb measurements, *Atmos Meas Tech*, 11, 2085-2100, doi.org//10.5194/amt-11-2085-2018, 2018.
- Mann, G. W., S. S. Dhomse, T. Deshler, C. Timmreck, A. Schmidt, R. Neely and L. Thomason: Evolving particle size is the key to improved volcanic forcings, *Past Global Change (PAGES) magazine*, 23, 52-52, 2015.
- Mills, M. J., Schmidt, A., Easter, R., Solomon, S., Kinnison, D. E., Ghan, S. J., Neely, R. R., Marsh, D. R., Conley, A.,  
450 Bardeen, C. G., and Gettelman, A.: Global volcanic aerosol properties derived from emissions, 1990-2014, using CESM1(WACCM), *Journal of Geophysical Research-Atmospheres*, 121, 2332-2348, doi.org/10.1002/2015jd024290, 2016.
- Rieger, L., Zawada, D. J., Bourassa, A., and Degenstein, D.: A multiwavelength retrieval approach for improved OSIRIS aerosol extinction retrievals, *J. Geophys. Res.*, 124, 7286-7307, 2019.
- Santer, B. D., Bonfils, C., Painter, J. F., Zelinka, M. D., Mears, C., Solomon, S., Schmidt, G. A., Fyfe, J. C., Cole, J. N. S.,  
455 Nazarenko, L., Taylor, K. E., and Wentz, F. J.: Volcanic contribution to decadal changes in tropospheric temperature, *Nature Geoscience*, 7, 185-189, doi.org/10.1038/Ngeo2098, 2014.
- Schmidt, A., and Robock, A.: Volcanism, the atmosphere, and climate through time, in: *Volcanism and Global Environmental Change*, edited by: Schmidt, A., Fristad, K. E., and Elkins-Tanton, L. T., Cambridge University Press, Cambridge, UK, 195-207, 2015.
- 460 Schmidt, A., Mills, M. J., Ghan, S., Gregory, J. M., Allan, R. P., Andrews, T., and al., e.: Volcanic radiative forcing from 1979 to 2015, *J. Geophys. Res.*, 123, 12,491– 412,508, doi.org//10.1029/2018JD028776, 2018.
- Solomon, S., Daniel, J. S., Neely, R. R., 3rd, Vernier, J. P., Dutton, E. G., and Thomason, L. W.: The persistently variable "background" stratospheric aerosol layer and global climate change, *Science*, 333, 866-870, doi.org/10.1126/science.1206027, 2011.
- 465 Stothers, R. B.: Major optical depth perturbations to the stratosphere from volcanic eruptions: Pyrheliometric period, 1881-1960, *Journal of Geophysical Research-Atmospheres*, 101, 3901-3920, doi.org/10.1029/95jd03237, 1996.
- Tang, Q., Hess, P., Brown-Steiner, B., and Kinnison, D.: Tropospheric ozone decrease due to the Mount Pinatubo eruption: Reduced stratospheric influx, *Geophys Res Lett*, 40, 5553-5558, doi.org//10.1002/2013GL056563, 2013.
- Thomason, L. W., Kent, G. S., Trepte, C. R., and Poole, L. R.: A comparison of the stratospheric aerosol background periods  
470 of 1979 and 1989-1991, *Journal of Geophysical Research-Atmospheres*, 102, 3611-3616, doi.org/10.1029/96jd02960, 1997a.



- Thomason, L. W., Poole, L. R., and Deshler, T.: A global climatology of stratospheric aerosol surface area density deduced from Stratospheric Aerosol and Gas Experiment II measurements: 1984-1994, *Journal of Geophysical Research-Atmospheres*, 102, 8967-8976, doi.org/10.1029/96jd02962, 1997b.
- 475 Thomason, L. W., Herber, A. B., Yamanouchi, T., and Sato, K.: Arctic study on tropospheric aerosol and radiation: comparison of tropospheric aerosol extinction profiles measured by airborne photometer and SAGE II, *Geophysical Research Letters*, 30, doi.org/10.1029/2002gl016453, 2003.
- Thomason, L. W., Burton, S. P., Luo, B. P., and Peter, T.: SAGE II measurements of stratospheric aerosol properties at non-volcanic levels, *Atmospheric Chemistry and Physics*, 8, 983-995, doi.org/10.5194/acp-8-983-2008, 2008.
- 480 Thomason, L. W., Moore, J. R., Pitts, M. C., Zawodny, J. M., and Chiou, E. W.: An evaluation of the SAGE III version 4 aerosol extinction coefficient and water vapor data products, *Atmospheric Chemistry and Physics*, 10, 2159-2173, 2010.
- Thomason, L. W., Ernest, N., Millán, L., Rieger, L., Bourassa, A., Vernier, J.-P., Manney, G., Luo, B., Arfeuille, F., and Peter, T.: A global space-based stratospheric aerosol climatology: 1979-2016, *Earth System Science Data*, 10, 469-492, 2018.
- Toohy, M., Stevens, B., Schmidt, H., and Timmreck, C.: Easy Volcanic Aerosol (EVA v1.0): an idealized forcing generator for climate simulations, *Geosci. Model Dev.*, 9, 4049-4070, doi.org/10.5194/gmd-9-4049-2016, 2016.
- 485 Vernier, J. P., Thomason, L. W., Pommereau, J. P., Bourassa, A., Pelon, J., Garnier, A., Hauchecorne, A., Blanot, L., Trepte, C., Degenstein, D., and Vargas, F.: Major influence of tropical volcanic eruptions on the stratospheric aerosol layer during the last decade, *Geophysical Research Letters*, 38, 12807, doi.org/10.1029/2011gl047563, 2011.
- Von Savigny, C., and Hofmann, C. G.: Issues related to the retrieval of stratospheric aerosol particle size information based on optical measurements, *Atmos Meas Tech*, 13, 1909-1920, doi.org/10.5194/amt-13-1909-1920, 2020.
- 490 Wang, P. H., Kent, G. S., McCormick, M. P., Thomason, L. W., and Yue, G. K.: Retrieval analysis of aerosol-size distribution with simulated extinction measurements at SAGE III wavelengths, *Applied Optics*, 35, 433-440, doi.org/10.1364/Ao.35.000433, 1996.
- Yue, G., and Deepak, A.: Retrieval of stratospheric aerosol size distribution from atmospheric extinction of solar radiation at two wavelengths, *Appl Opt*, 22, 1639-1645, 1983.